

A. Aria Tzika
Richard L. Robertson
Patrick D. Barnes
Sridhar Vajapeyam
Patricia E. Burrows
S. Ted Treves
R. Michael Scott

Childhood moyamoya disease: hemodynamic MRI

Received: 20 February 1996
Accepted: 4 February 1997

Presented at the 38th Annual Meeting
of the Society for Pediatric Radiology,
Washington, DC, 27–30 April 1995

A. A. Tzika (✉) · R. L. Robertson ·
P. D. Barnes · S. Vajapeyam ·
P. E. Burrows · S. T. Treves
Department of Radiology,
Children's Hospital and
Harvard Medical School,
300 Longwood Avenue,
Boston, MA 02115, USA

Abstract *Background.* Childhood moyamoya disease is a rare progressive cerebrovascular disease.

Objective. To evaluate cerebral hemodynamics using dynamic Gd-DTPA-enhanced imaging in children with moyamoya disease. *Materials and methods.* Eight children (2–11 years of age) with the clinical and angiographic findings typical of moyamoya disease, before and/or after surgical intervention (pial synangiosis), underwent conventional MR imaging (MRI) and hemodynamic MR imaging (HMRI). HMRI used a spoiled gradient-echo with low flip angle (10 deg) and long TE (TR/TE = 24/15 ms) to minimize T1 effects and emphasize T2* weighting. Raw and calculated hemodynamic images were reviewed. Three-dimensional

time-of-flight MR angiography (MRA) and perfusion brain single photon emission computed tomography (SPECT) were also performed.

Results. Abnormal hemodynamic maps resulting from vascular stenosis or occlusion and basal collaterals were observed in six patient studies. HMRI depicted perfusion dynamics of affected cerebrovascular territories, detected cortical perfusion deficits, and complemented conventional MRI and MRA. HMRI findings were consistent with those of catheter angiography and perfusion SPECT.

Conclusion. Our preliminary experience suggests that HMRI may be of value in the preoperative and postoperative evaluation of surgical interventions in moyamoya disease.

Introduction

Moyamoya disease is a rare and progressive cerebrovascular disease of unknown etiology. The highest prevalence is reported in Japan [1]. Definitive diagnosis is made by catheter angiography, which reveals steno-occlusive disease at the internal carotid artery bifurcation and a characteristic “moyamoya” or “puff of smoke” angiographic appearance representing extensive net-like collateral vessels within the basal ganglia and thalami [2]. Childhood moyamoya disease differs from the adult form in that the disease typically occurs bilaterally, the moyamoya vessels are more prominent, there is a higher incidence of symptomatic ischemia, and there is a lower incidence of intracranial bleeding and aneu-

rysms [3, 4]. Differences in the site and frequency of infarction as observed by magnetic resonance imaging (MRI) have also been reported [5]. The current surgical treatment in our institution is pial synangiosis in which the superficial temporal artery (STA) is attached surgically to the pia. The goal of surgical revascularization is to preserve neurologic function by restoring vascular supply to the ischemic brain through the generation of transpial collaterals derived from the STA [6]. Using a bolus gadolinium-enhanced T2*-weighted MR technique, we hypothesize that by imaging cerebral hemodynamics, which are directly related to brain function, we could complement the current neuroimaging evaluation of children with moyamoya disease, including those undergoing surgery [7, 8].

Materials and methods

Subjects

Eight patients, five girls and three boys (ages 2–11 years), with one or more episodes of cerebral ischemia and moyamoya disease as diagnosed by catheter angiography, also underwent conventional MRI, MR angiography (MRA) and hemodynamic MRI (HMRI) on a 1.5-T imaging system with a quadrature head coil (Signa; GE Medical Systems, Milwaukee, Wis.). We performed a total of nine examinations, including two preoperative and seven postoperative evaluations. Postoperative studies were performed 1 year after bilateral pial synangiosis [6]. The findings on all HMRI studies were compared with the angiographic, MRI and MRA results. The results of five HMRI studies were also compared with the findings from perfusion single photon emission computed tomography (SPECT).

MRI protocol

The MRI protocol included: T1- and T2-weighted conventional MRI, 3D time-of-flight MRA, HMRI and T1-weighted, Gd-DTPA-enhanced MRI.

Conventional MRI

MRI was performed using conventional spin-echo sagittal T1-weighted images (TR = 600 ms, TE = 20 ms, NEX 2, 24 cm field of view, 5 mm slice thickness with a 20% interslice gap, and 128 × 256 acquisition matrix), fast spin-echo proton density-weighted images (TR = 2000 ms, TE = 17 ms, NEX 1, 24 cm field of view, 5 mm slice thickness with a 50% interslice gap, 192 × 256 acquisition matrix, echo train length = 4), and fast spin-echo T2-weighted images (TR = 3200 ms, TE = 85 ms, NEX 1, 24 cm field of view, 5 mm slice thickness with a 50% interslice gap, 192 × 256 acquisition matrix, echo train length = 8).

MR angiography

MRA was performed using a 3D time-of-flight sequence with the following parameters: TR = 40 ms, flip angle = 20 deg, TE = 6.9 ms, NEX 1, 18 cm field of view, 6 cm volume with 1 mm partition thickness, 128 × 256 acquisition matrix. A saturation band was placed above the imaged volume to decrease venous flow signal.

Hemodynamic MRI

HMRI was performed using a spoiled gradient-echo (SPGR) sequence during an intravenous bolus injection of 0.1 mmol/kg Gadoteridol or Prohance (Squibb Diagnostics, Bristol-Myers Squibb, Princeton, N.J.), with the following parameters: TR = 24 ms, TE = 15 ms, flip angle = 10 deg, NEX 0.75, 26 cm field of view, 10 mm slice thickness, 128 × 256 acquisition matrix. Thirty images were acquired consecutively every 2.5 s at one anatomical level selected from the conventional MR images. The first six images are collected in order to achieve equilibrium with the pulse sequence. The contrast is injected after the sixth image and the image acquisition continues until all 30 images are acquired. The procedure lasts 1 min 25 s and allows for the transit of the contrast through the brain. In our experience, this time is adequate to account for delays in perfusion of certain vascular territories in patients with cerebrovascular disorders.

Table 1 Angiographic staging of moyamoya disease (adapted with modification from Suzuki and Takaku [10])

Stage	Angiographic findings
1	Narrowing of internal carotid artery bifurcation without collaterals
2	Initiation of moyamoya collaterals
3	Intensification of moyamoya collaterals
4	Minimization of moyamoya collaterals
5	Reduction of moyamoya collaterals
6	Disappearance of moyamoya collaterals

The MR images were transferred from the Signa to a Sun SPARCStation 10 computer (Sun Microsystems, Mountain View, Calif.) over an Ethernet, where data analysis procedures were performed using a program written in C, and percent signal intensity images and hemodynamic parameter maps were generated [9]. The procedure for the hemodynamic parameter calculation is as follows: a noise threshold value, obtained from the known noise level of the MR scanner, is used to generate a mask image to suppress background noise. For each pixel above the noise threshold, an average precontrast signal intensity (SI_0) is calculated. For each pixel within the mask, the concentration or $\Delta R2^*(t) = [\ln(SI_0/SI(t))]/TE$, where $SI(t)$ is the signal intensity at time "t", and the $\Delta R2^*(t)$ versus t curves are obtained for each pixel. Hemodynamic parameter maps of interest are then generated as follows: the relative cerebral blood volume (rCBV) map, which is the area under the $\Delta R2^*$ peak calculated by pixelwise numerical integration, the mean transit time (MTT) map calculated from the effective width of the $\Delta R2^*$ peak, and the cerebral blood flow map, which is the ratio of the area under the $\Delta R2^*(t)$ peak to the difference between the MTT and the mean bolus injection time, calculated on a pixelwise basis. For each raw image acquired, the program also calculates a percent signal intensity image, which is the intensity distribution across the selected slice as a percentage of the average precontrast intensity distribution, calculated on a pixel-by-pixel basis for each image. The percent signal intensity images suppress the precontrast signal intensity distribution across the slice and reflect only the signal intensity changes caused by the bolus transit.

Catheter angiography

All patients underwent conventional catheter angiography prior to surgery. Six patients were studied by angiography 1 year following synangiosis. Angiography was performed with general anesthesia in children under 10 years of age, and with sedation and local anesthesia in older children. Standard femoral arterial catheterization with a modified Seldinger technique and systemic heparinization were used. Selective contrast medium injections were made in the internal and external carotid arteries bilaterally, and in one or both vertebral arteries. Filming was carried out using a serial digital subtraction technique. In seven of eight cases, the angiogram was performed within 1 week of the MRI, MRA and HMRI examinations. In the eighth patient, a preoperative angiogram performed at another institution was used for correlation. The images were evaluated by a neuroradiologist (R. L. R.) and graded according to the extent and severity of the stenocclusive involvement, including moyamoya collaterals, using a previously described staging scheme (Table 1) [4, 10]. Basal ganglia and transpial collaterals were qualitatively graded as minor (+), moderate (++) , or extensive (+++) (Table 2).

Table 2 Qualitative analysis of HMRI findings from eight patients with moyamoya disease (RICA right internal carotid artery, LICA left internal carotid artery, N/A not assessed)

Patient no. age (years) sex operative status	Vessels	Angiographic stage	Basal ganglia collaterals	Transspial collaterals ^a	MRA stage	MRI findings	HMRI findings	SPECT findings
1 2, F Preoperative	RICA	3	+++ (R)	N/A	3	Chronic right parietal and frontal and left parieto-occipital infarctions; flow voids due to basal ganglia collaterals	Right frontal cortical perfusion deficit; bilateral parieto-occipital deficits; basal ganglia collaterals	Right frontal cortical perfusion deficit; bilateral parieto-occipital deficits
	LICA	3	++ (L)	N/A	3			N/A
2 6, M Preoperative	RICA	3	+++ (R)	N/A	N/A	New bilateral frontal, right head of caudate, and right putaminal foci of T2 prolongation	Bilateral cortical perfusion deficits; basal ganglia collaterals; no transspial collaterals	N/A
	LICA	3	+++ (L)	N/A	3	Left frontal lobe lacunar infarction; flow voids due to basal ganglia collaterals	Frontal cortical perfusion asymmetry; left cortical perfusion deficit; basal ganglia collaterals	Left hemispheric hypoperfusion; mostly frontal, temporal, parietal
3 4, F Postoperative	RICA	3	+++ (R)	+++ (R)	N/A	Chronic high right fronto-parietal infarction; a few flow voids due to basal ganglia collaterals	No perfusion deficit at lower level than T2 signal abnormality on MRI; no basal ganglia collaterals; (+) transspial collaterals	Extensive right frontoparietal deficit
	LICA	4	++ (L)	+++ (L)	N/A			deficit
4 11, F Postoperative	RICA	3	+(R)	+++ (R)	4	Right head of caudate infarction with foci of T2 prolongation in the frontal white matter bilaterally; no flow voids in basal ganglia	No detectable cortical perfusion deficit; no basal ganglia collaterals; (+) transspial collaterals	N/A
	LICA	6	LICA occluded proximally	+++ (L)	6			N/A
5 11, F Postoperative	RICA	3	+++ (R)	+(R)	N/A	Right and small left frontal infarctions; flow voids due to basal ganglia collaterals	Right frontal cortical deficit; good MCA territory perfusion; slight left parieto-occipital cortical deficit; basal ganglia and transspial collaterals	N/A
	LICA	4	++ (L)	++ (L)				
6 11, F Postoperative	RICA	1	+(R)	+++ (R)	N/A	Wide left sylvian fissure; minimal flow voids due to basal ganglia collaterals	No perfusion deficits; no basal ganglia collaterals; (+) transspial collaterals	N/A
	LICA	4	+(L)	+++ (L)				
7 4, M Postoperative	RICA	3	+++ (R)	+++ (R)	3	Evolution of a right temporoparietal infarction; flow voids due to basal ganglia collaterals	Delayed and reduced frontal cortical perfusion; no apparent temporoparietal perfusion deficit at this level; mild basal ganglia collaterals; (+) transspial collaterals	Reduced tracer localization in the region of temporal parietal infarct
	LICA	5	+(L)	+++ (L)	5			
8 7, F Postoperative	RICA	3	++ (R)	+++ (R)	3	No MR signal abnormalities; minimal flow voids due to basal ganglia collaterals	No perfusion deficits; early flow in the temporal region; mild basal ganglia collaterals; (+) transspial collaterals	Bilaterally symmetric perfusion
	LICA	3	+++ (L)	+++ (L)	3			

^a As qualitatively evaluated from the right (R) or left (L) cerebral angiograms: + minor, ++ moderate, +++ extensive

Perfusion brain SPECT

For perfusion brain SPECT, technetium-99m (^{99m}Tc) bismate (Neurolite, DuPont Merck, Billerica, Mass.) was given intravenously approximately 2 h prior to imaging. Tracer injections were performed while the patient rested comfortably in a quiet environment for at least 5 min. The dosage of ^{99m}Tc -bismate was 0.3 mCi (11.1 MBq)/kg, with a minimal dose of 1.0 mCi (37 MBq), and a maximal dose of 20 mCi (740 MBq).

SPECT images were obtained using a triple detector system (MultiSPECT 3, Siemens Gammasonics, Hoffman Estates, Ill.) equipped with ultra-high-resolution collimators. A magnification zoom of 1.45 was used. Each detector rotated 360° around the patient's head in 40 nonoverlying stops of 30 s each. Hence, a total of 120 images were obtained in 20 min. Reconstruction was conducted using filtered back projection and a Butterworth filter. Cheng's attenuation correction was applied to the studies.

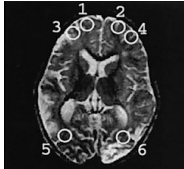
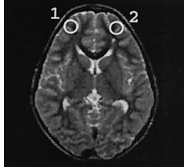
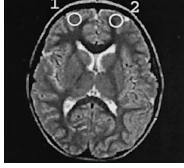

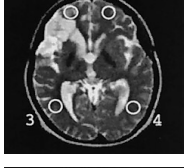
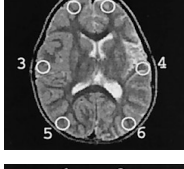

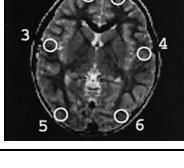
Results

Table 2 summarizes the qualitative analysis of the angiographic, MRA, MRI, HMRI and SPECT findings. Table 3 summarizes regions-of-interest (ROI) analysis on selected cortical regions from the same patients as in Table 2. The calculated contralateral ratios of approximately 1 indicated symmetrical cortical perfusion.

Angiographically, the disease was bilateral in all cases. The moyamoya or basal ganglia collaterals were extensively developed unilaterally or bilaterally in six out of eight patients (patients 1, 2, 3, 5, 7, 8). Transpial collaterals as a result of the pial synangiosis were present in all postoperative patients (patients 3–8). Extensive transpial collaterals were present bilaterally in five patients (patients 3, 4, 6, 7, 8). In one patient (patient 5), transpial collaterals were graded angiographically as moderate on the left and minor on the right. Staging by catheter angiography and MRA were in agreement in all but one case (patient 4) in which MRA overestimated the severity of obstruction.

MRI showed evidence of infarction in all but one case (patient 8). HMRI showed reduced hemodynamics at all lesion sites detected by MRI. In four cases (patients 1, 2, 3 and 7), HMRI detected frontal cortical perfusion deficits in the absence of MRI abnormality. Decreased blood flow to these regions was confirmed by angiography. HMRI detected deficits or asymmetries in four cases: two preoperatively (patients 1, 2; Fig. 1, 2) and two postoperatively (patients 5, 7; Fig. 3, 4). The other four patients (patients 3, 4, 6, 8) presented symmetrical ROIs (Table 3). In the postoperative patients, only frontal deficits were identified and the other cerebral territories were bilaterally well perfused. Postoperative patients (patients 3–8) exhibited symmetric cortical perfusion with one exception (Table 1). Only one case (patient 5) demonstrated persistent frontal and occipital hemodynamic asymmetries (Tables 2, 3).

Table 3 Quantitative analysis of HMRI data from eight patients with moyamoya disease. The ROIs used in this analysis, determined from T2-weighted MR images shown here, included primarily brain parenchyma. The intensity measurements were determined from the same locations in the HMRI images. The mean intensity value and the standard deviation from 177 pixels were established

1	1:2	0.71	
	3:4	0.77	
	5:6	0.80	
2	1:2	1.75	
3	1:2	1.1	
4	1:2	0.94	
	3:4	0.99	
	5:6	1.11	
5	1:2	1.69	
	3:4	1.36	
6	1:2	1.15	
	3:4	0.99	
	5:6	1.18	
7	1:2	0.87	
	3:4	0.97	
8	1:2	0.96	
	3:4	1.01	
	5:6	1.16	

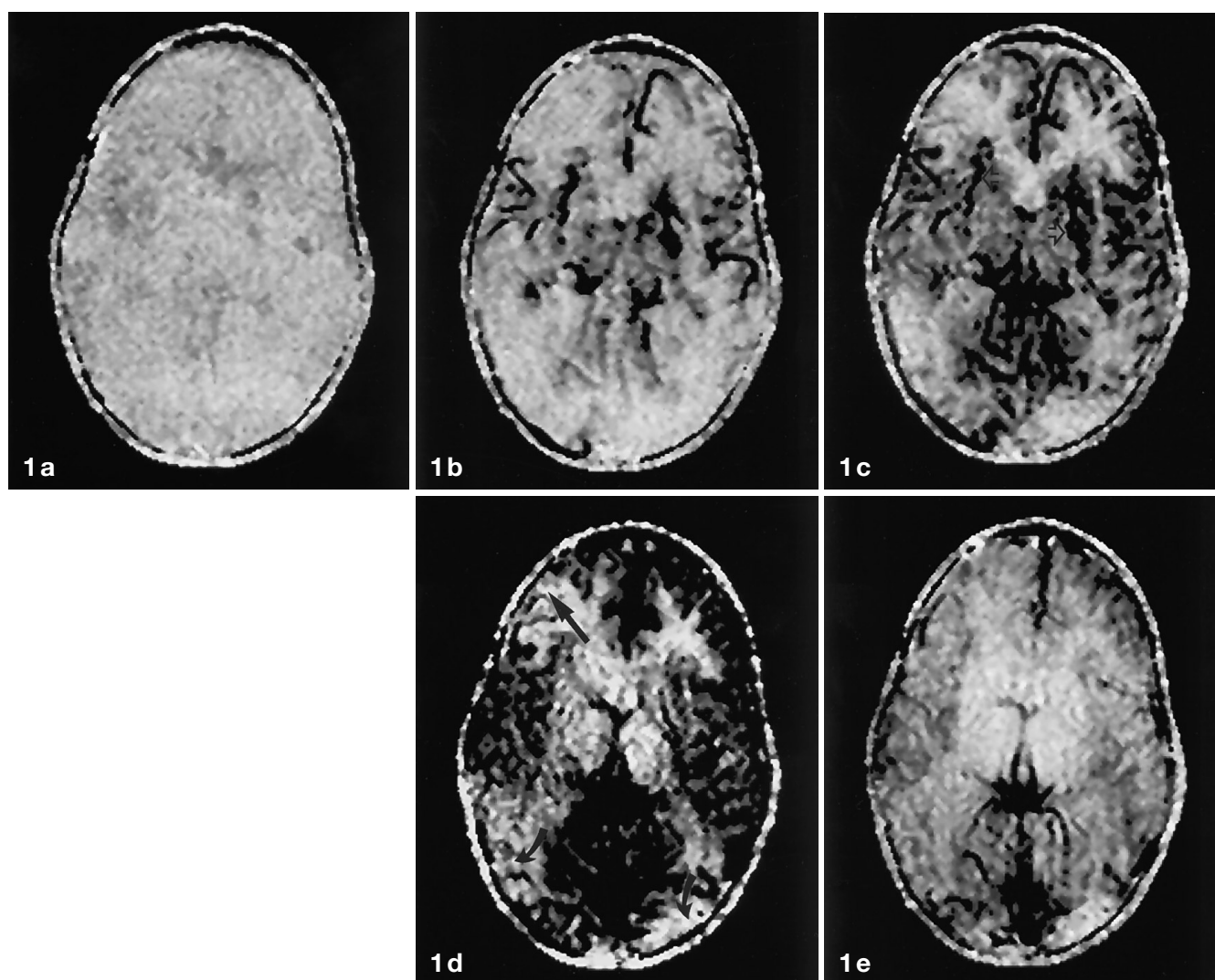


Fig 1a-e Untreated moyamoya disease in a 2-year-old girl (patient 1). Percent signal intensity change with bolus transit through the brain. Images **a** (baseline) to **e** (10.0 s) show the intensity distribution across the selected slice as related to the transit of Gd-DTPA at intervals of 2.5 s as a percentage of the average prebolus intensity distribution calculated on a pixel-by-pixel basis. Perfusing areas show a drop in signal intensity and appear darker, whereas hypoperfusing regions do not darken during bolus transit. Note the reduced perfusion in the right frontal cortical region (*straight arrow*) compared to the left, and the perfusion deficits in the parieto-occipital cortices bilaterally (*curved arrows*). Also note prominent early perfusion of the basal ganglia due to moyamoya collaterals (*open arrows*)

Basal ganglia collaterals were detected angiographically in varying degrees in all patients (Table 2). These collaterals produced flow voids in the basal ganglia and were detected by MRI in all but one case in which mild collateral circulation was shown by cerebral angiography (patient 4, Table 2). HMRI detected basal ganglia collat-

erals in all but two cases (patients 3, 4, Table 2). HMRI demonstrated transpial collaterals to the middle cerebral artery territory bilaterally in the six patients studied 1 year following synangiosis (patients 3-8, Table 2).

SPECT findings were in spatial agreement with the HMRI findings in five cases (patients 1, 2, 3, 7, 8). Post-operative SPECT results were not available in three patients.

Discussion

MRI is sensitive to the structural cerebrovascular abnormalities of moyamoya disease. Findings suggesting the diagnosis on MRI include multiple infarctions, absent or diminished vascular flow voids in the circle of Willis and prominent flow voids in the basal ganglia. MRA complements MRI by showing more clearly the vessels involved [11, 12].

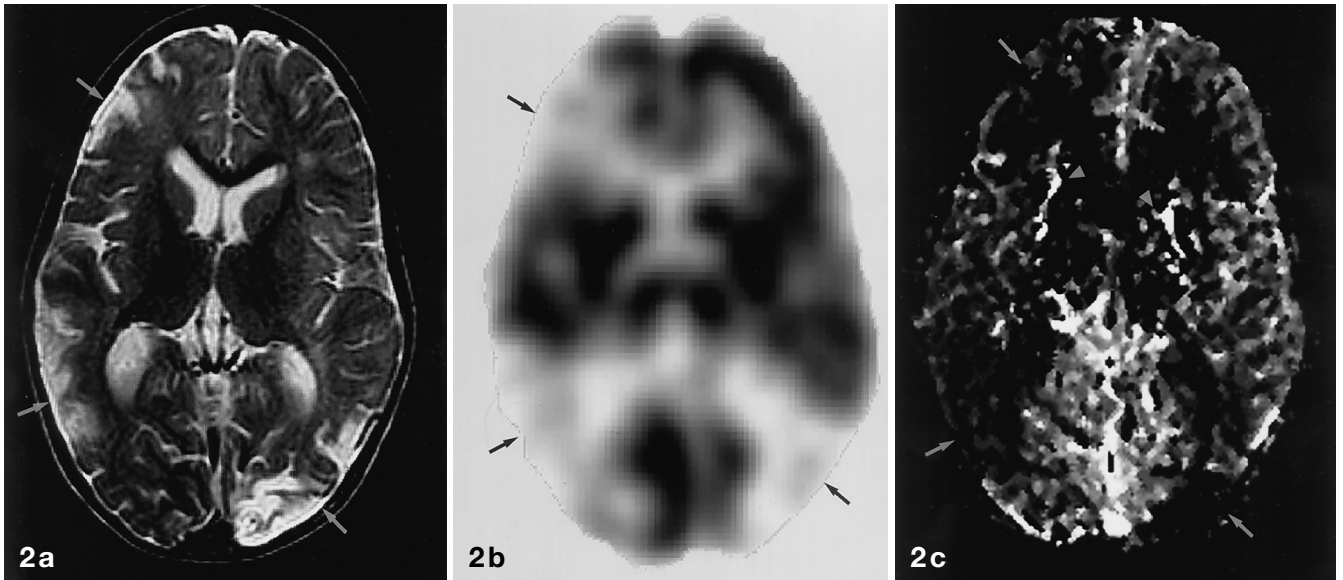


Fig. 2 a-c MRI, SPECT and HMRI of the same patient as in Fig. 1. **a** This T2-weighted MR image shows chronic right parietal and frontal and left parieto-occipital infarctions (arrows) and cortical atrophy. **b** Perfusion SPECT reveals absence of perfusion of the right frontal cortex and bilateral parieto-occipital cortices (arrows). **c** This blood volume calculated HMRI image represents a calculated hemodynamic map from a 10-mm-thick brain slice with darker areas showing regions of lower relative cerebral blood volume. The image exhibits diminished perfusion of the right frontal cortex and bilateral parieto-occipital cortices (arrows) and increased perfusion in the lentiform nuclei (arrowheads)

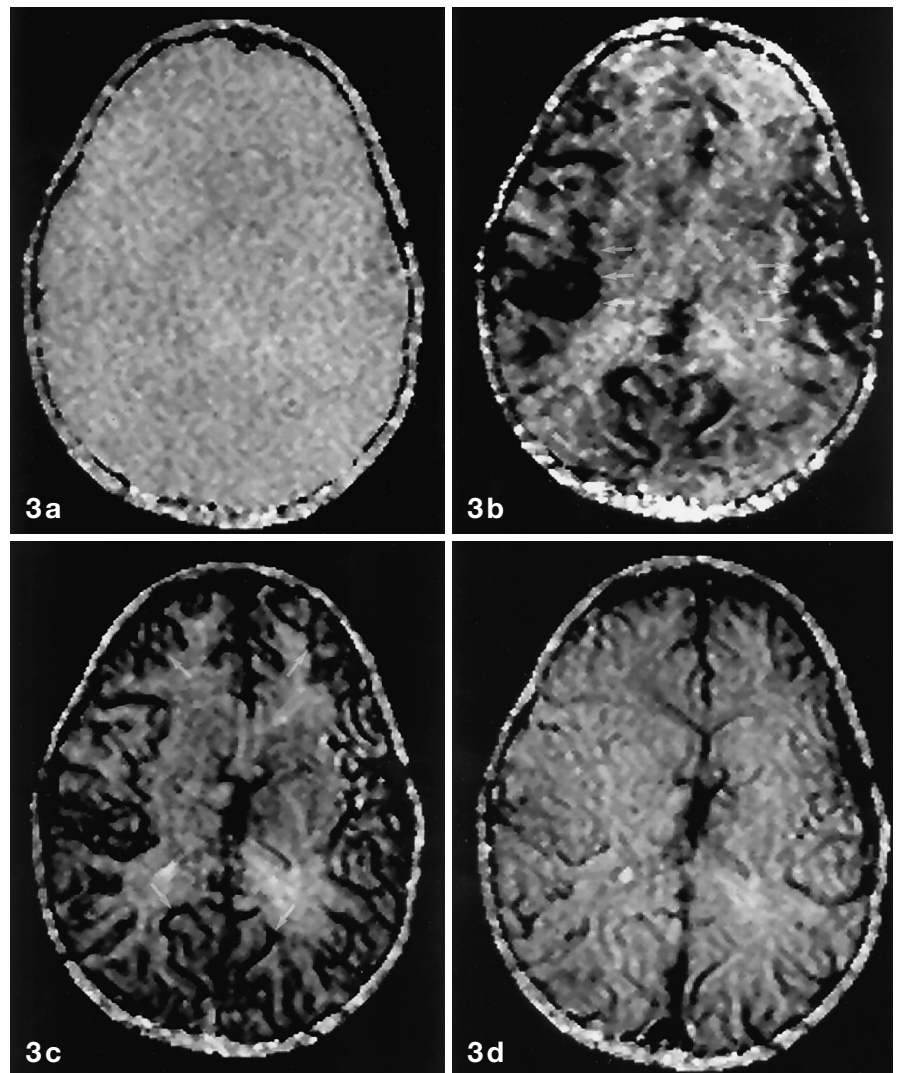


Fig. 3 a-d One year after bilateral pial synangiosis in a 11-year-old girl (patient 6). Percent signal intensity change with bolus transit through the brain. Images **a-d** show the percent signal intensity distribution across the slice as related to the transit of the Gd-DTPA bolus through the brain from baseline (**a**) to 7.5 s (**d**). Note that the perisylvian territory perfuses early (**b**), followed by the frontal and occipital cortical areas (**c**). The basal ganglia do not show prominent perfusion due to poorly developed moyamoya collaterals

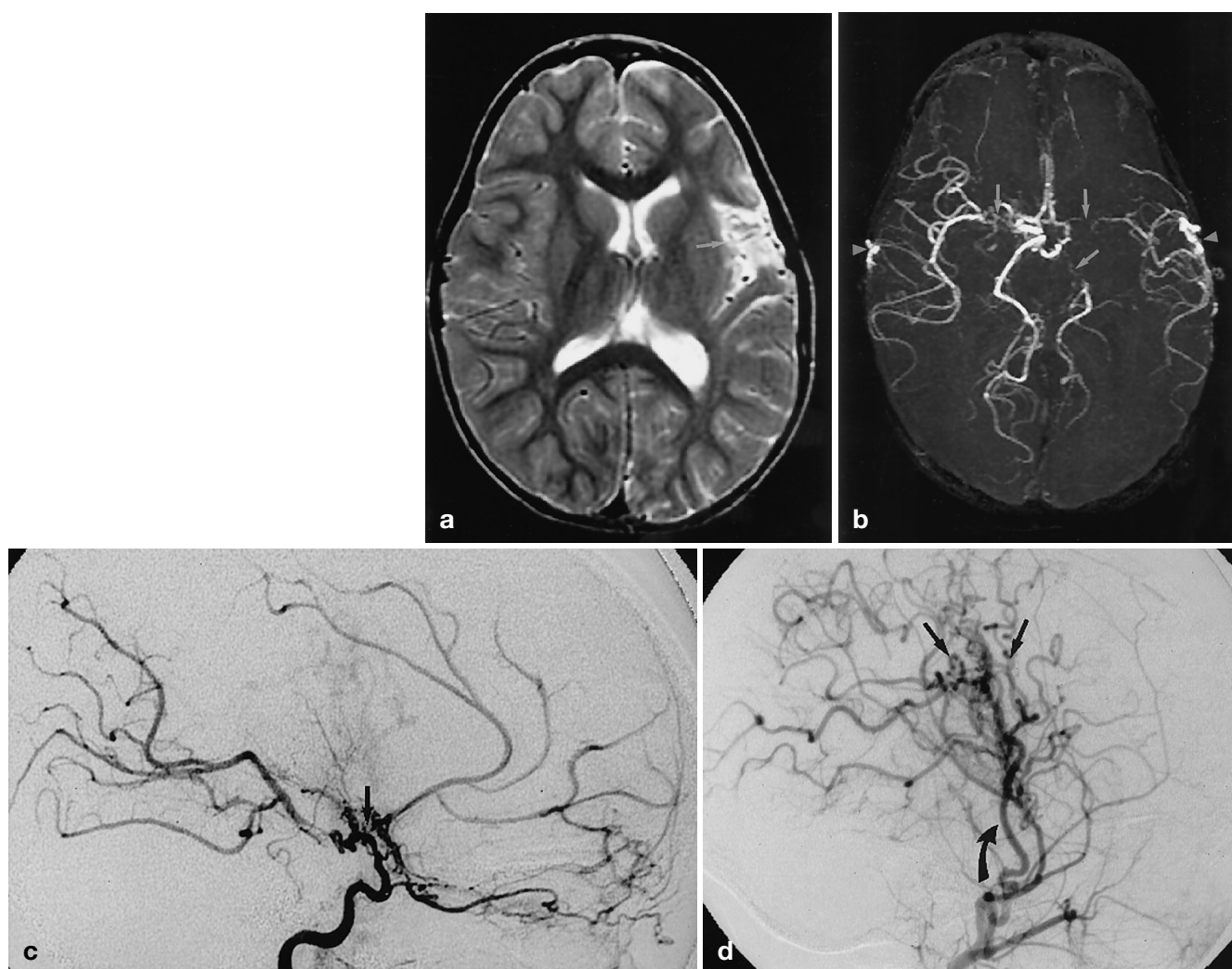


Fig 4a-d MRI, MRA and angiography of the same patient as in Fig.3. Conventional T2-weighted MRI (**a**) and MRA (**b**) are shown along with digital subtracted angiography (**c, d**). **a** The T2-weighted MR image depicts a wide left sylvian fissure (*arrow*) related to prior distal MCA infarction. **b** The MRA shows reduced flow enhancement consistent with severe stenosis or occlusion of the MCAs bilaterally and of the left PCA (*arrows*). There is flow-related enhancement in the STA bilaterally (*arrowheads*). **c** On the lateral ICA injection, occlusion of the supraclinoid left ICA (*arrow*) is shown. **d** On the lateral external carotid injection, well-developed transpial collaterals from the STA (*curved arrow*) to the MCA are demonstrated (*arrows*)

In this study, we used a dynamic T2*-weighted MR technique which has been previously described [8, 13–15]. Our approach to HMRI consists of rapid imaging of a Gd-DTPA bolus transit through the brain using a T2*-weighted MR pulse sequence. A bolus of a susceptibility contrast agent distorts the local magnetic field homogeneity (shortens T2*) and results in dephasing

of spins and signal loss. In our T2*-weighted images (Figs.1, 3), perfused tissue appears hypointense or “dark” due to the short T2* of perfusing protons. Perfusion deficit regions appear hyperintense or “bright” due to the long T2* protons. Thus, the pattern of contrast enhancement on the dynamic contrast-enhanced T2*-weighted images is different from that in T1-weighted images and reflects primarily blood volume distribution. The theory underlining the mechanism of contrast enhancement has been experimentally approached and reviewed elsewhere [16–19].

Several limitations of the HMRI technique currently used must be mentioned. First, only a single 10-mm-thick slice can be imaged repetitively every 2.5 s. This provides adequate temporal resolution of the bolus transit through the brain but does not permit functional evaluation of the entire brain. When available, faster gradients combined with echo planar techniques can be used to image the entire brain efficiently, thus overcoming this limitation [20]. Secondly, quantification of abso-

lute values for hemodynamic parameters is needed [21]. Preliminary data have shown promise and good agreement with positron emission tomography (PET), but further evaluation is needed [22].

In seven moyamoya patients, abnormal hemodynamic maps on HMRI were supported by matching MRA and angiographic findings of arterial occlusion, stenosis and collateral formation. In one patient (patient 3, Table 2), HMRI did not detect any major basal ganglia collateral perfusion. The discrepancy between the HMRI and angiographic findings may be due to the selection of the anatomic level for HMRI, which did not include the basal ganglia territory in its entirety. It can also be attributed to the low resolution of the HMRI using the current methodology. This discrepancy may be resolved in the near future with the use of a three-dimensional technique. HMRI was in agreement, however, with SPECT at a similar anatomical level in one of the cases. SPECT was not performed in the other case.

The angiographic grading systems previously proposed for moyamoya disease are based on the severity and location of arterial stenosis and the degree of basal ganglia collaterals [3, 4]. These grading systems present limitations in correlating regional cerebral perfusion with grade, since they neither take into account transpial or transdural collaterals (surgical or native) derived from the external carotid artery nor consider the posterior circulation involvement. While external carotid collaterals may be relatively unimportant in early moyamoya disease, they become more significant with disease progression and after surgical synangiosis. We have tried to assess qualitatively the angiographic demonstration of transpial collaterals separate from our angiographic grading.

As a result of surgically created transpial collaterals as confirmed angiographically, HMRI showed bilaterally symmetric cortical perfusion in four of six patients (patients 3, 4, 6, and 8; Tables 2, 3). In patient 5, perfusion deficits as evaluated by HMRI (Tables 2, 3) were in agreement with angiographic findings of minor and moderate transpial collateralization from the right and left synangioses respectively. Although extensive transpial collaterals were formed, patient 7 exhibited reduced and delayed frontal cortical perfusion which was attributed to poor frontal lobe circulation as revealed on angiography.

Underperfused regions were distinguished from perfused cerebral territories. The overall perfusion pattern was in good spatial agreement with SPECT (Table 2). Figures 1, 2 (patient 1) and Figs. 3, 4 (patient 6) illustrate cerebral perfusion dynamics in two typical patients before and following pial synangiosis respectively. This type of information is independent and complementary to MRI because it is based on cerebral hemodynamics [13], which are directly related to brain function [23]. For example, the atrophic cortical regions shown in pa-

tient 1 (Fig. 2 a) exhibit perfusion deficits as identified in the dynamic images (Fig. 1 a–e). Also the rCBV map (Fig. 2 c) was in good agreement with the SPECT image (Fig. 2 b). Postoperative exams in patient 6 showed the success of pial synangiosis by demonstrating the distribution of the collateral circulation developed from the STA. This information was not available from the MRI. The dynamic images (Fig. 3 a–d) exhibit excellent bilateral perfusion which is symmetric according to selected intensity ratios (Table 3). The atrophied left parietal cortex, as indicated by the bright signal in the T2-weighted image (Fig. 4 a), shows good hemodynamics (Fig. 3 a–d), although MRA shows severe bilateral MCA and left PCA stenosis or occlusion. Thus, vascular supply to the originally ischemic cortex is provided largely by the collaterals developed from the STA and middle meningeal artery following the procedure of pial synangiosis 1 year earlier. This was confirmed by the findings on angiography, which showed well-developed collaterals derived from the external carotid artery branches (Fig. 4 c–d). This case is illustrative of the complementary value of HMRI to conventional MRI and MRA.

Our results with HMRI agree with published observations of the hemodynamic changes in moyamoya disease using PET. Investigators have found reduced blood flow to the affected hemisphere and significantly increased blood volume in the lentiform nuclei [24]. This is illustrated in Fig. 1 b–d, where the affected cortices exhibit diminished perfusion and blood flow is increased to the lentiform nuclei. Also, the blood volume map (Fig. 2 c) shows decreased blood volume (dark) in the affected cortices and increased blood volume (bright) in the lentiform nuclei bilaterally. It has been reported that hemodynamic changes depend on the stage of the disease. Using ^{133}Xe , cerebral blood flow of the frontal lobes has been found to be decreased [25, 26]. We have observed similarly low perfusion in the frontal lobes of our moyamoya patients (Table 1). In fact, HMRI has the ability to detect hemodynamic changes in the frontal cortex which are not apparent with MRA because of small vessel dynamics.

The capability of this technique to provide information on hemodynamics not available from conventional MRI and MRA, and the potential for demonstrating the pathophysiologic characteristics of stroke, as well as guiding early therapeutic intervention, has been reported in some pediatric and adult patients [15].

In conclusion, HMRI provides additional functional information not available from conventional MRI, MRA, or angiography. HMRI may be of value in the preoperative and postoperative evaluation of surgical intervention in moyamoya disease.

Acknowledgements We thank our nurses and technologists for their assistance. We also appreciate the support and encouragement of the chairman of the Department of Radiology, Donald R. Kirks.

References

1. Takeuchi K, Shimizu K (1957) Hypoplasia of the bilateral internal carotid arteries. *Brain Nerve* 9: 37–43
2. Ueki K, Meyer F, Mellinger J (1994) Moyamoya disease: the disorder and surgical treatment. *Mayo Clin Proc* 69: 749–757
3. Satoh S, Shibuya H, Matsushima Y, Susuki S (1988) Analysis of the angiographic findings in cases of childhood moyamoya disease. *Neuroradiology* 30: 111–119
4. Suzuki J, Kodama N (1983) Moyamoya disease – a review. *Stroke* 14: 104–109
5. Takanashi J, Sugita K, Ishii M, et al (1993) Moyamoya syndrome in young children: MR comparison with adult onset. *AJNR* 14: 1139–1143
6. Adelson P, Scott R (1995) Pial synangiosis for moyamoya syndrome in children. *Pediatr Neurosurg* 23: 26–33
7. Rosen B, Belliveau J, Chien D (1989) Perfusion imaging by nuclear magnetic resonance. *Magn Reson Q* 5: 263–281
8. Tzika A, Massoth R, Ball W, Majumdar S, Dunn R, Kirks D (1993) Cerebral perfusion in children: detection with dynamic contrast-enhanced T2*-weighted MR images. *Radiology* 187: 449–458
9. Liu W-C, Massoth R, Tzika A, Dunn R, Ball W (1993) Automation for MRI-derived hemodynamic parameter analysis. In: *Proceedings of the Society of Magnetic Resonance in Medicine*. Society of Magnetic Resonance, Berkeley, Calif, 714
10. Suzuki J, Takaku A (1969) Cerebrovascular “moyamoya” disease. Disease showing abnormal net-like vessels in base of the brain. *Arch Neurol* 20: 288–299
11. Maas K, Barkovich A, Dong L, Edwards M, Picuch R, Charlton V (1994) Selected indications for and applications of magnetic resonance angiography in children. *Pediatric Neurosurg* 20: 113–125
12. Yamada I, Suzuki S, Matsushima Y (1995) Moyamoya disease: comparison of assessment with MR angiography and MR imaging versus conventional imaging. *Radiology* 196: 211–218
13. Rosen B, Belliveau JW, Vevea JM, Brady TJ (1990) Perfusion imaging with NMR contrast agents. *Magn Reson Med* 14: 249–265
14. Edelman RR, Mattle HP, Atkinson DJ, et al (1990) Cerebral blood flow: assessment with dynamic contrast-enhanced T2*-weighted MR imaging at 1.5 T. *Radiology* 176: 211–220
15. Warach S, Li W, Ronthal M, Edelman RR (1992) Acute cerebral ischemia: evaluation with dynamic contrast-enhanced MR imaging and MR angiography. *Radiology* 182: 41–47
16. Belliveau JW, Rosen BR, Kantor HL, et al (1990) Functional cerebral imaging by susceptibility-contrast NMR. *Magn Reson Med* 14: 538–546
17. Villringer A, Rosen BR, Belliveau JW, et al (1988) Dynamic imaging with lanthanide chelates in normal brain: contrast due to magnetic susceptibility effects. *Magn Reson Med* 6: 164–174
18. Wendland MF, White DL, Aicher KP, Tzika AA, Moseley ME (1991) Detection with echo-planar MR imaging of transit of susceptibility contrast medium in a rat model of regional brain ischemia. *JMRI* 1: 285–292
19. White DL, Aicher KP, Tzika AA, Kucharczyk J, Engelstad BL, Moseley ME (1992) Iron-dextran as a magnetic susceptibility contrast agent: flow-related contrast effects in the T2-weighted spin-echo MRI of normal rat and cat brain. *Magn Reson Med* 24: 14–28
20. Edelman R, Siewert B, Darby D, et al (1994) Qualitative mapping of cerebral blood flow and functional localization with echo-planar MR imaging and signal targeting with alternating radio frequency. *Radiology* 192: 513–520
21. Massoth R, Tzika A, Dunn R, Liu W-C, Majumdar S, Ball W (1993) Validation of hemodynamic parameters obtained from dynamic Gd-DTPA enhanced T2*-weighted MRI (abstr). In: *Proceedings of the Society of Magnetic Resonance in Medicine*. Society of Magnetic Resonance, Berkeley, Calif, 392
22. Rempp K, Gunnar B, Wenz F, Becker C, Gückel F, Lorenz W (1994) Quantification of regional cerebral blood flow and volume with dynamic susceptibility contrast-enhanced MR imaging. *Radiology* 193: 637–641
23. Roy CS, Sherrington CS (1890) On the regulation of the blood-supply of the brain. *J Physiol (Lond)* 11: 85–109
24. Tomura N, Kanno I, Shishido F, et al (1989) Vascular responses in cerebrovascular “moyamoya” disease evaluated by positron emission tomography. *No To Shinkei* 41: 895–904
25. Takeuchi S, Tanaka R, Ishii R, Tsuchida T, Kobayashi K, Arai H (1985) Cerebral hemodynamics in patients with moyamoya disease. A study of regional blood flow by the ¹³³Xe inhalation method. *Surg Neurol* 23: 468–474
26. Ogawa A, Nakamura N, Sakurai Y, Kayama T, Wada T, Suzuki J (1987) Cerebral blood flow in moyamoya disease. (in Japanese) *No To Shinkei* 39: 199–203